Paleoceanography and Paleoclimatology

RESEARCH ARTICLE
10.1029/2021PA004394

Key Points:

- Evidence of Southern Ocean surface warming and West Antarctic Ice Sheet mass loss during Marine Isotope Stage-31 is observed
- Obliquity pacing of warmth is observed in the northern Antarctic Zone of the Southern Ocean (AZSO); precession pacing is observed in the south
- Warm conditions are observed in the northern AZSO thousands of years before the south

Supporting Information:

Supporting Information may be found in the online version of this article.

Correspondence to:

J. P. Warnock,
jwarnock@iup.edu

Citation:

Warnock, J. P., Reilly, B. T., Raymo, M. E., Weber, M. E., Peck, V., Williams, T., et al. (2022). Latitudinal variance in the drivers and pacing of warmth during mid-Pleistocene MIS 31 in the Antarctic zone of the Southern Ocean. *Paleoceanography and Paleoclimatology*, *37*, e2021PA004394. https://doi.org/10.1029/2021PA004394

Received 16 NOV 2021
Accepted 16 JUL 2022

Latitudinal Variance in the Drivers and Pacing of Warmth During Mid-Pleistocene MIS 31 in the Antarctic Zone of the Southern Ocean

Jonathan P. Warnock[1], Brendan T. Reilly[2], Maureen E. Raymo[3], Michael E. Weber[4], Victoria Peck[5], Trevor Williams[6], Linda Armbrecht[7], Ian Bailey[8], Stefanie Brachfeld[9], Zhiheng Du[10], Gerson Fauth[11], Marga M. García[12], Anna Glüder[13], Michelle Guitard[14], Marcus Gutjahr[15], Sidney Hemming[3], Iván Hernández-Almeida[16], Freida S. Hoem[17], Ji-Hwan Hwang[18], Mutsumi Iizuka[19], Yuji Kato[20], Bridget Lee[21], Yasmina M. Martos[22,23], Suzanne O'Connell[24], Lara F. Pérez[5,25], Thomas A. Ronge[26], Osamu Seki[27], Lisa Tauxe[2], Shubham Tripathi[28], Xufeng Zheng[29], Joseph Stoner[13], and Reed P. Scherer[30]

[1]Department of Geography, Geology, Environment and Planning, Indiana University of Pennsylvania, Indiana, PA, USA, [2]Scripps Institution of Oceanography, University of California, San Diego, La Jolla, CA, USA, [3]Lamont-Doherty Earth Observatory, Columbia University, Palisades, NY, USA, [4]Department of Geochemistry and Petrology, University of Bonn, Institute for Geosciences, Bonn, Germany, [5]British Antarctic Survey, Cambridge, UK, [6]International Ocean Discovery Program, Texas A&M University, College Station, TX, USA, [7]Institute for Marine and Antarctic Studies (IMAS), University of Tasmania, Hobart, TAS, Australia, [8]Camborne School of Mines and Environmental Sustainability Institute, University of Exeter, Penryn Campus, Cornwall, UK, [9]Earth and Environmental Studies, Montclair State University, Montclair, NJ, USA, [10]State Key Laboratory of Cryospheric Sciences, Chinese Academy of Sciences, Lanzhou Gansu, China, [11]Geology Program, University of Vale do Rio dos Sinos, Instituto Tecnologico de Micropaleontologia, San Leopoldo, Brazil, [12]Cádiz Oceanographic Center, Spanish Institute of Oceanography, Cádiz, Spain, [13]College of Earth, Ocean and Atmospheric Sciences, Oregon State University, Corvallis, OR, USA, [14]College of Marine Science, University of South Florida, St. Petersburg, FL, USA, [15]GEOMAR Helmholtz Centre for Ocean Research Kiel, Kiel, Germany, [16]Department of Earth Sciences, ETH Zürich, Switzerland, [17]Marine Palynology and Paleoceanography, Utrecht University, Utrecht, The Netherlands, [18]Earth and Environmental Sciences, Korea Basic Science Institute, Chungbuk Cheongju, Republic of Korea, [19]Knowledge Engineering, Tokyo City University, Tokyo, Japan, [20]Faculty of Life and Environmental Sciences, University of Tsukuba, Ibaraki, Japan, [21]Department of Earth Sciences, University of California, Riverside, CA, USA, [22]NASA Goddard Space Flight Center, University of Maryland System, Greenbelt, MD, USA, [23]Department of Astronomy, University of Maryland, College Park, MD, USA, [24]Department of Earth and Environmental Sciences, Wesleyan University, Middletown, CT, USA, [25]Department of Marine Geology, Geological Survey of Denmark and Greenland, Aarhus, Denmark, [26]Marine Geology, Alfred-Wegener-Institute Hemholtz-Center for Polar and Marine Research, Bremerhaven, Germany, [27]Institute for Low Temperature Science, Hokkaido University, Sapporo Hokkaido, Japan, [28]National Centre for Polar and Ocean Research, Ministry of Earth Sciences, Vasco da Gama, India, [29]State Key Laboratory of Marine Resource Utilization in South China Sea, Hainan University, Haikou, China, [30]Department of Earth, Atmosphere and Environment, Northern Illinois University, DeKalb, IL, USA

Abstract Early Pleistocene Marine Isotope Stage (MIS)-31 (1.081–1.062 Ma) is a unique interval of extreme global warming, including evidence of a West Antarctic Ice Sheet (WAIS) collapse. Here we present a new 1,000-year resolution, spanning 1.110–1.030 Ma, diatom-based reconstruction of primary productivity, relative sea surface temperature changes, sea-ice proximity/open ocean conditions and diatom species absolute abundances during MIS-31, from the Scotia Sea (59°S) using deep-sea sediments collected during International Ocean Discovery Program (IODP) Expedition 382. The lower Jaramillo magnetic reversal (base of C1r.1n, 1.071 Ma) provides a robust and independent time-stratigraphic marker to correlate records from other drill cores in the Antarctic Zone of the Southern Ocean (AZSO). An increase in open ocean species *Fragilariopsis kerguelensis* in early MIS-31 at 53°S (Ocean Drilling Program Site 1,094) correlates with increased obliquity forcing, whereas at 59°S (IODP Site U1537; this study) three progressively increasing, successive peaks in the relative abundance of *F. kerguelensis* correlate with Southern Hemisphere-phased precession pacing. These observations reveal a complex pattern of ocean temperature change and sustained sea surface temperature increase lasting longer than a precession cycle within the Atlantic sector of the AZSO. Timing of an inferred WAIS collapse is consistent with delayed warmth (possibly driven by sea-ice dynamics) in the southern AZSO, supporting models that indicate WAIS sensitivity to local sub-ice shelf melting. Anthropogenically enhanced

impingement of relatively warm water beneath the ice shelves today highlights the importance of understanding dynamic responses of the WAIS during MIS-31, a warmer than Holocene interglacial.

Plain Language Summary Sea level rise and other impacts resulting from loss of ice from the Antarctic Ice Sheet due to climate change are a significant societal concern. Studying past periods of ice loss can help to predict future ice loss and understand the types of conditions that result in massive ice loss. Marine Isotope Stage 31, a past period of significant Antarctic ice loss, is studied using diatoms, fossil algae. Evidence of sea surface warming leading to Antarctic ice loss is identified. These data also reveal a more complex timing of warming than has been previously recognized across the Southern Ocean. Warmth affects the northern parts thousands of years before more southerly regions. Additionally, northern parts of the Southern Ocean are seen to be controlled by different orbitally driven climate factors than southern parts. The study highlights the importance of warm Southern Ocean water on future ice mass loss.

1. Introduction

The response of the Antarctic Zone of the Southern Ocean (AZSO; south of the Polar Front), and the Antarctic Ice Sheets (AIS) to rapid warming is of increasing scientific concern in light of anthropogenic-driven global warming (Gilbert & Kittel, 2021). One key effort has been identifying and analyzing geologically recent warm periods as potential partial analogs for ongoing, anthropogenically enhanced changes. In particular, records from periods of significant East (EAIS) and West Antarctic Ice Sheet (WAIS) mass loss are sought to understand the sequence of events involved in ice sheet collapse, the consequences for the world's oceans to Antarctic ice mass loss and to reconstruct rates of sea surface temperature change and sea-level rise. Two hypotheses have been put forward to explain AIS mass loss during the Pliocene and early Pleistocene. Huybers (2006) suggested that the obliquity-paced (~40 kyr) summer melt period had the primary control on ice mass loss, resulting in the obliquity-controlled benthic $\delta^{18}O$ isotope record. In contrast, Raymo et al. (2006) suggested that local precession forcing (paced at ~20 kyr) holds significant influence over AIS mass balance, and that the apparent dominance of obliquity in the global benthic $\delta^{18}O$ isotope record is a result of the northern and southern hemisphere precession-driven component of ice volume signals being out of phase, and thus largely canceling each other in the globally mixed $\delta^{18}O$ records. Many authors have invoked warm water upwelling at the marine-based grounding line of the WAIS as a mechanism for ice volume loss (Morlighem et al., 2020; Nakayama et al., 2014; Raymo et al., 2006; Rignot et al., 2013; Seroussi et al., 2017; Weber et al., 2014), highlighting the importance of studying past WAIS behavior and WAIS/CDW (circumpolar deep water) interaction.

Marine Isotope Stage (MIS-) 31, 1.081 to 1.062 Ma (Lisiecki & Raymo, 2005), has received much attention as a "super interglacial" (Melles et al., 2012) and a period of possible WAIS collapse and EAIS ice volume reduction (DeConto et al., 2012; Scherer et al., 2008). Furthermore, MIS-31 is geologically "recent" and hence a good analog warm period to today due to its similarity in tectonic and oceanographic configuration (Maldonado et al., 2014). Although other Pleistocene interglacials, notably MIS-11, also have been considered "super interglacials," MIS-31 is an anomalously warm interglacial of the pre-100 kyr cycle, with biomarker-based summer sea surface temperature estimates of 5 ± 1.2°C warmer than modern (Beltran et al., 2019). Furthermore, while the precessional component is different, MIS-31 has an insolation and eccentricity configuration somewhat similar to today. MIS-31 also has similar insolation orbital configuration to other more recent interglacials, MIS-11 and MIS-5, with the difference that the former shows higher obliquity and eccentricity coinciding with a precession minimum. This configuration led to some of the highest high latitude summer insolation levels of the Pleistocene (Laskar et al., 2004). Despite relatively high atmospheric CO_2 concentrations during MIS-31 (Hönisch et al., 2009), the AIS had greater mass during MIS-31, than MIS-11 (Elderfield et al., 2012). Even with differences from modern, and other warm "super interglacials," MIS-31 provides an instructive case-study to learn about climate sensitivity of the EAIS and WAIS.

Most importantly, peak northern hemisphere insolation of MIS-31 precisely coincides with the lower Jaramillo normal polarity subchron transition (Channell et al., 2008; Horng et al., 2002; Scherer et al., 2008; Shackleton et al., 1990), making it possible to unambiguously identify and correlate MIS-31 events in sediment cores with reliable paleomagnetic records (Reilly et al., 2021), even if they lack benthic $\delta^{18}O$ data. It is this lack of oxygen isotope-based, orbitally tuned chronologies that remains a significant challenge to studying past climate records, especially in the SO. Utilizing the lower Jaramillo paleomagnetic reversal, the precision chronostratigraphy used

in this study thus allows reliable analysis of lead/lag relationships of oceanographic events across the SO as well as globally.

Multiple records of SO warming during MIS-31 have been published. Scherer et al. (2008) used diatom and coccolithophore fossils recovered from a distal, more open AZSO site (Ocean Drilling Program (ODP) Site 1,094) and a proximal, sea-ice influenced, Antarctic continental shelf site (Cape Roberts Project Site CRP-1) to identify a circum-Antarctic period of greatly reduced sea-ice extent and likely ice shelf loss during MIS-31. They found precession pacing of warmth and suggested that marine-based sectors of the AIS may be more susceptible to warming and high insolation than had been widely recognized. Maiorano et al. (2009) presented calcareous nannofossil evidence of warming greater than that seen during other interglacials over MIS-31 at ODP Site 1,090. The position of the polar front was north of Site 1,090 during MIS-31, further indicating warmth (Cartagena-Sierra et al., 2021). EAIS retreat, at least in the vicinity of Prydz Bay (ODP Site 1,165), is supported by nannofossil evidence (Villa et al., 2008), however, continued iceberg-rafting indicates that the EAIS and its marine-terminating glaciers remained capable of shedding icebergs through MIS-31 (Teitler et al., 2015). The ANtarctic DRILLing project (ANDRILL) drillcore AND-1B, recovered MIS-31 sediments from beneath the McMurdo Ice Shelf of the Ross Sea, which revealed open water conditions from MIS-31 to MIS-27 (McKay et al., 2012), and suggested a complete collapse of the McMurdo Ice Shelf over both warm and cold MIS stages (Naish et al., 2009; Scherer et al., 2007; Villa et al., 2012). An ice sheet-shelf model, as well as global climate model simulations, support a loss of ice shelves and a large ice sheet response, with significant loss of the marine-based WAIS and some retreat of the EAIS ice during MIS-31 (Beltran et al., 2019; DeConto et al., 2012). Consistency between model simulations and observations indicating the absence of the Ross Ice Shelf, as well as Pleistocene age diatoms consistent with (though not limited to) MIS-31 recovered from beneath the WAIS (Scherer et al., 1998) provide compelling evidence that the WAIS collapsed during MIS-31 (DeConto et al., 2012). More recent modeling efforts, combined with biomarker analysis, suggest direct insolation forcing led to a shorter sea-ice season, poleward intensification of the westerlies, and warm CDW intrusion to the continental shelf during MIS-31 (Beltran et al., 2019). This led to an estimated 5°C warming of the sea surface in the AZSO relative to modern in the AZSO, a temperature not considered consistent with a marine-grounded WAIS (Beltran et al., 2019). Here we utilize sediments from IODP Site U1537 to evaluate diatom-derived sea surface temperature change during MIS-31 in order to understand the potential timing, magnitude, and duration of WAIS mass loss.

1.1. Regional Setting

The sediments analyzed in this study were recovered during IODP Expedition 382, "Iceberg Alley and Subantarctic Ice and Ocean Dynamics," which recovered Scotia Sea sediments at sites U1536, U1537 (Dove Basin) and U1538 (Pirie Basin) (Figure 1). IODP Site U1537 is located in the Dove Basin of the Scotia Sea, 59°6.65′S, 40°54.37′W in a water depth of 3,713 m (Weber et al., 2021). Icebergs shed from around Antarctica pass through the Dove Basin, giving this area the name "Iceberg Alley" (Anderson & Andrews, 1999). Icebergs melt when they interact with warm water of the Antarctic Circumpolar Current, releasing terrigenous sediment to the seafloor and providing nutrients in the upper water column (Budge & Long, 2018). Site U1537 is located on a contourite deposit under the influence of AABW, with sediments consisting of diatom ooze and diatom-bearing silty clay (Pérez et al., 2021; Weber et al., 2021). High sedimentation rates up to 100 cm/kyr make this area ideal for recovering high resolution records of Antarctic and Southern Ocean change (Weber et al., 2012). Samples were taken from Holes *A* and *D* of Site U1537 following its primary splice (stratigraphic composite section depths from different holes to create as continuous as possible record).

2. Materials and Methods

2.1. Diatom Methods

Diatom slide preparation followed the method of Warnock and Scherer (2014). This method allows for the generation of species relative abundance data (%) as well as absolute diatom abundance (ADA) in valves per gram dry weight of sediment (v/gdw). In addition, diatom species' absolute abundances, as valves per gram dry weight of sediment, were calculated for U1537. An Olympus BX 53 microscope with oil immersion and Nomarski differential interference contrast operating at 1,000*x* magnification was used for all diatom counts. Each slide

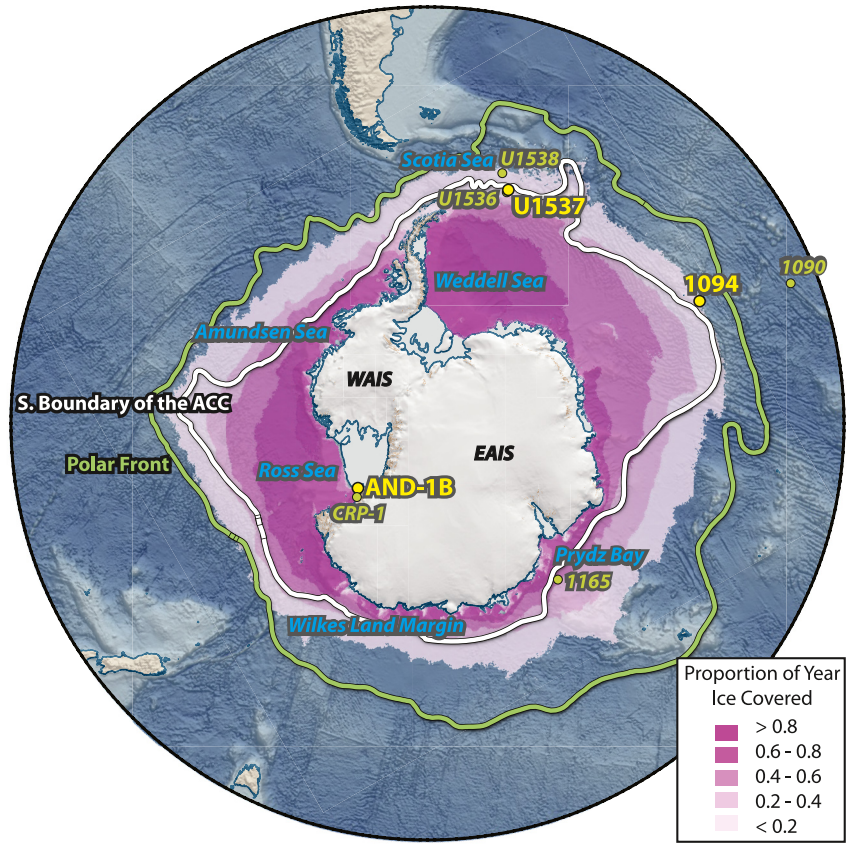

Figure 1. Site locations, including International Ocean Discovery Program Expedition 382 Site U1537, Ocean Discovery Program Leg 177 Site 1,094, ANtarctic DRILLing Site AND-1B (yellow), along with Cape Roberts Project-1 and select other circum Antarctic records (green) that contain Marine Isotope Stage-31 sediments. Purple shading indicates the proportion sea-ice coverage during the year, based on data from 2002 to 2011 (Spreen et al., 2008). Colored lines indicate the position of the southern boundary of the Antarctic Circumpolar Current (white) and Polar Front (green) (Orsi et al., 1995). Map created with Quantarctica (Matsuoka et al., 2021), using ETOPO1, IBSCO, and RAMP2 data (Amante & Eakins, 2009; Arndt et al., 2013; Liu et al., 2015). AP = Antarctic Peninsula; WAIS = West Antarctic Ice Sheet; EAIS = East Antarctic Ice Sheet.

was counted until 300 non-*Chaetoceros* resting spore (CRS) diatom valves had been identified, or a maximum of three complete transects were analyzed across a 40 mm wide coverslip. CRS were excluded from the 300 diatom valve tally because they can dominate diatom assemblages, thereby considerably biasing count data toward CRS at the expense of including rarer, but environmentally predictive, diatoms in the analysis. However, CRS were added to the total diatom count upon completing the counts for each slide, such that they were included in the overall relative species abundance and ADA calculations.

Taxonomic authorities are provided in Table S1 in Supporting Information S1. Individual diatom species were assigned to ecological affiliations (sea-ice, open ocean, and subtropical) based on Armand et al. (2005), Crosta et al. (2005), and Romero et al. (2005), which were also used by Scherer et al. (2008). The extinct species *Thalassiosira elliptipora* was considered part of the open ocean group, following Scherer et al. (2008). In addition, *Eucampia antarctica* was associated with the sea-ice group to make a direct comparison to Scherer et al. (2008) who considered it a sea ice affiliated species. Species ecological associations are provided in Table S2. Diatoms were analyzed at a ~1,000-year resolution, with 71 unique intervals analyzed through the section.

2.2. Age Model

The age model for Site U1537 through the analyzed time interval (Reilly et al., 2021) is constrained by the positions of three magnetic reversals, the boundaries of the Jaramillo Subchron (C1r.1n; 990–1,071 ka, in MIS-27 and -31) and the top of the Cobb Mountain Subchron (top C1r.2n; 1,187 ka, in MIS-35; Channell et al., 2008).

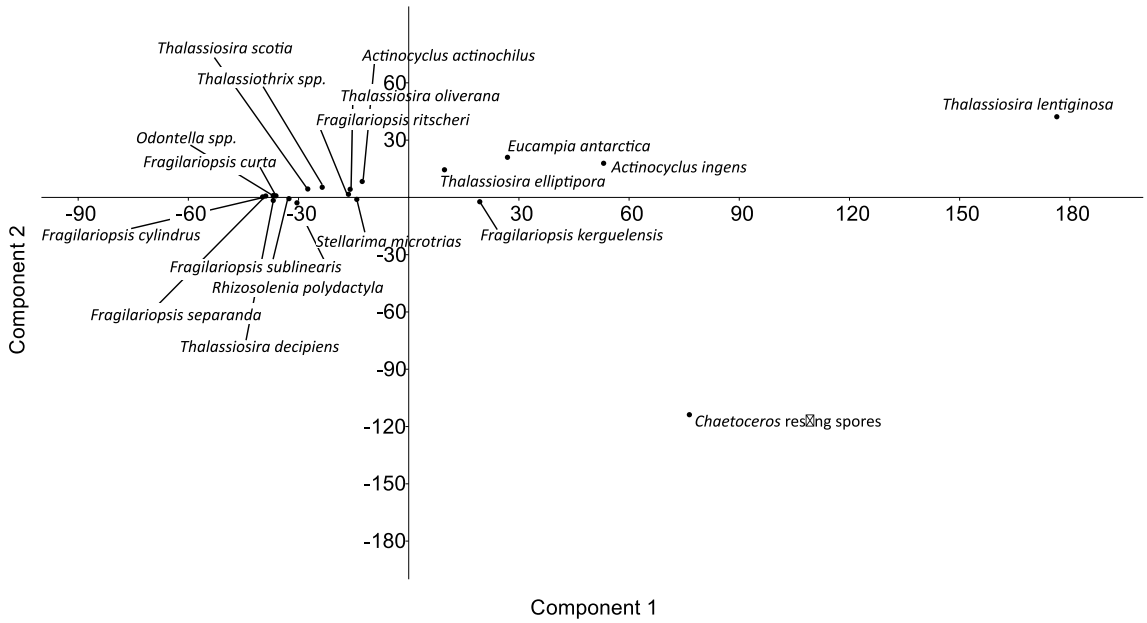

Figure 2. Principle components analysis performed using relative abundance data of any species with an abundance of at least 3% in a single sample. The analysis was performed using the software package PAST (Hammer et al., 2001). Spp. = species. The axes represent Principle component analysis scores.

Age-depth uncertainties between these tie points are estimated using Undatable MATLAB tools and an *xfactor* of 0.1 (Lougheed & Obrochta, 2019). No additional tie points were used in the age model; hence, uncertainty in age increases with distance in the depth-domain from the reversals. The lower Jaramillo magnetic reversal at site 1,094 is associated with the minimum in benthic $\delta^{18}O$ stratigraphies recording MIS-31 (Channell et al., 2008; Horng et al., 2002; Shackleton et al., 1990). In Expedition 382 records (Site U1537 and nearby Site U1536) the base of the reversal occurs in the same position relative to lithologic changes between diatom ooze and diatom-bearing silty clays, with no evidence of stratigraphic discontinuities, giving further confidence in identification of a complete MIS-31 (see Figure S4 in Reilly et al., 2021). A potentially higher precision age model for this time interval has been presented for Site U1537 using the assumption that magnetic susceptibility variations as well as *x*-ray fluorescence counts of Ca and Fe are synchronous with glacial-interglacial variability defined by the LR04 benthic isotope stack (Weber et al., 2022). This new age model by Weber et al. (2022) falls within the larger uncertainty structure of the Reilly et al. (2021) magnetostratigraphic age model. For this study we plot our data on the median age of the magnetostratigraphic age model, as the two age models are largely similar in this time interval and this decision requires fewer assumptions about the phasing of climate signals in the Early Pleistocene. However, we acknowledge that, while accurate, this age model has lower overall precision and, accordingly, we plot age uncertainty estimates in our summary figure (Figure 4).

2.3. Statistics

Principle component analysis (PCA) was used to identify relationships among diatom species. Furthermore, PCA was used to reduce the dimension of the biological data set, and to detect underlying factors driving the species' distributions in the ordination space. PCA was performed using the software package PAST v. 3.10 (Hammer et al., 2001). Initially, PCA was run using data from all observed species. However, many of these species make up an insignificant part of the record, and when plotted created a dense cluster of overlapping taxa that was impossible to resolve in graphical form. Therefore, PCA was run using the relative abundances of all species that constituted at least 3% of the assemblage in at least one sample. The following species met this criterion and were used in the PCA: *Actinocyclus actinochilus, Actinocyclus ingens,* CRS, *E. antarctica, Fragilariopsis curta, Fragilariopsis cylindrus, Fragilariopsis kerguelensis, Fragilariopsis ritscheri, Fragilariopsis separanda, Fragilariopsis sublinearis, Odontella* spp., *Rhizosolenia polydactyla, Stellarima microtrias, Thalassiosira decipiens, Thalassiosira elliptopora, Thalassiosira lentiginosa,Thalassiosira oliverana, Thalassiosira scotia* and *Thalassiothrix* spp. (Figure 2).

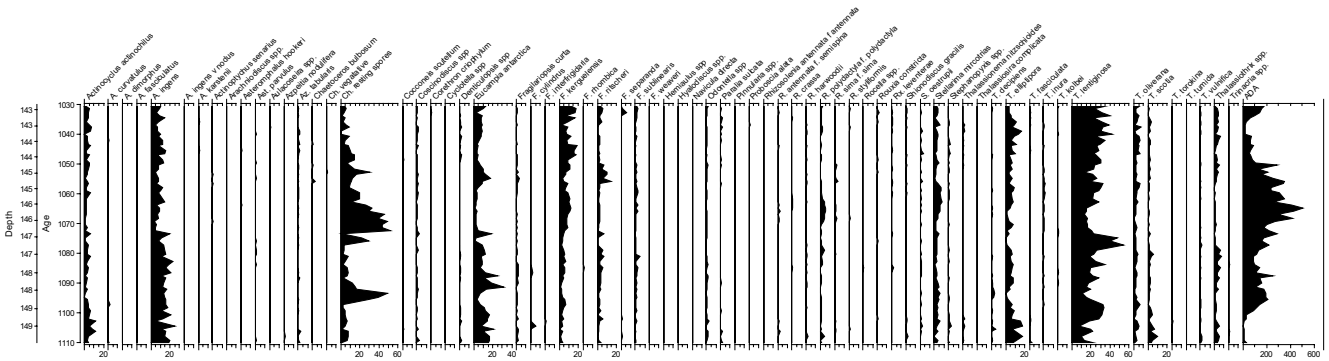

Figure 3. All diatom species data. All diatom species relative abundances (%) are plotted against depth and time. In addition, absolute diatom abundance is plotted as valves per gram dry weight of sediment. *A.* = *Actinocyclus*, *Ast.* = *Asteromphalus*, *Az.* = *Azpeitia*, *Ch* = *Chaetoceros*, *F.* = *Fragilariopsis*, *R.* = *Rhizosolenia*, *Rx.* = *Rouxia*, *S.* = *Shionodiscus*, *T.* = *Thalassiosira*.

3. Results

Diatoms occur in all 71 analyzed samples from Site U1537 in the Scotia Sea (Figure 3). ADA values range from 1.27×10^6 to 2.53×10^7 v/gdw (valves per gram dry weight). *Th. lentiginosa,* CRS, *A. ingens, E. antarctica*, *F. kerguelensis*, *Th. elliptipora* and are the dominant taxa in the studied interval (Table S2). CRSs are episodically abundant, with relative abundance ranging from 0% to 52.3% of the assemblage. It is worth noting, however, that during intervals of high abundance CRS contribute nearly as much as *Th. lentiginosa.*

The relative abundance of CRS (%CRS) displays three distinct peaks, which are visually consistent with NH-precession-paced variation (Figure 4g; orbital data sourced from Laskar et al., 2004). Peak 2 (centered at ~1.070 Ma) is the broadest and highest of the CRS relative abundance peaks and spans ~10,000 years. It coincides with the lower Jaramillo paleomagnetic reversal, which corresponds to the interval when and just after benthic $\delta^{18}O$ values are at their lowest during MIS-31 (Figures 4a and 4c). Furthermore, northern hemisphere insolation peaks at this point (Figure 4h). ADA follows a similar "3 peak" pattern and has similar variability to wet-bulk density (Figures 3, 4a, 4b). In each case, the highest ADA values occur slightly after a maximum in %CRS is reached. Relative abundance of *F. kerguelensis,* the most common open ocean diatom in the modern Southern Ocean, follows the three-peak trend of ADA and also lags the relative abundance peaks of CRS (Figure 4g). Open ocean affiliated *Th. elliptipora* abundance is similar to that of *F. kerguelensis*; however, the amplitude of the peaks is lower (Figure 3). In contrast, open ocean affiliated *Th. lentiginosa*, which represents 8%–54% of the assemblage, consistently peaks before the ADA and *F. kerguelensis* peaks (Figure 3). Sea-ice related species (e.g., *E. antarctica* and *F. curta*; Figures 4e and 4f) and relatively warm open ocean species (e.g., *F. kerguelensis* and *Th. lentiginosa*) abundances are negatively correlated. The relative abundance of CRS is generally seen to increase at the transitions between sea-ice dominated assemblages (Figure 4g) and open ocean dominated assemblages (Figure 4d).

Diatom absolute abundance data (valves of each species per gram dry weight of sediment) present a somewhat different pattern compared to relative abundance data (%; Figure 5). CRS, *F. kerguelensis* and *Th. lentiginosa* represent the species with the highest absolute abundances (Figure 5). Absolute abundance data show a much greater contrast between low diatom accumulation glacials and high accumulation interglacials. MIS 32 is characterized by low abundance, with one peak of CRS, *F. kerguelensis* and *Th. lentiginosa* occurring around 1.070 Ma. *Th. lentiginosa* increases its absolute abundance rate early in MIS-31, whereas absolute abundances of CRS and *F. kerguelensis* peak in the latter half of MIS-31. Interestingly, *Th. lentiginosa* maintains its high abundance into MIS-30, declining slowly until ~1.050 Ma, whereas absolute abundances of CRS and *F. kerguelensis* both decline more quickly at the onset of MIS-31. CRS achieve a slight absolute abundance peak at ~1.052 Ma. All three species reach their glacial low absolute abundance values at approximately 1.049 Ma. Absolute abundance rates for these species remain low until very late MIS-30. The single data point available shows continued increase in MIS-29.

The first PCA axis explains 68.7% of the variance in the data. On the far positive end of this axis we find *Th. lentiginosa*. In decreasing order, CRS, *A. ingens, E. antarctica, F. kerguelensis and Th. elliptipora* have positive

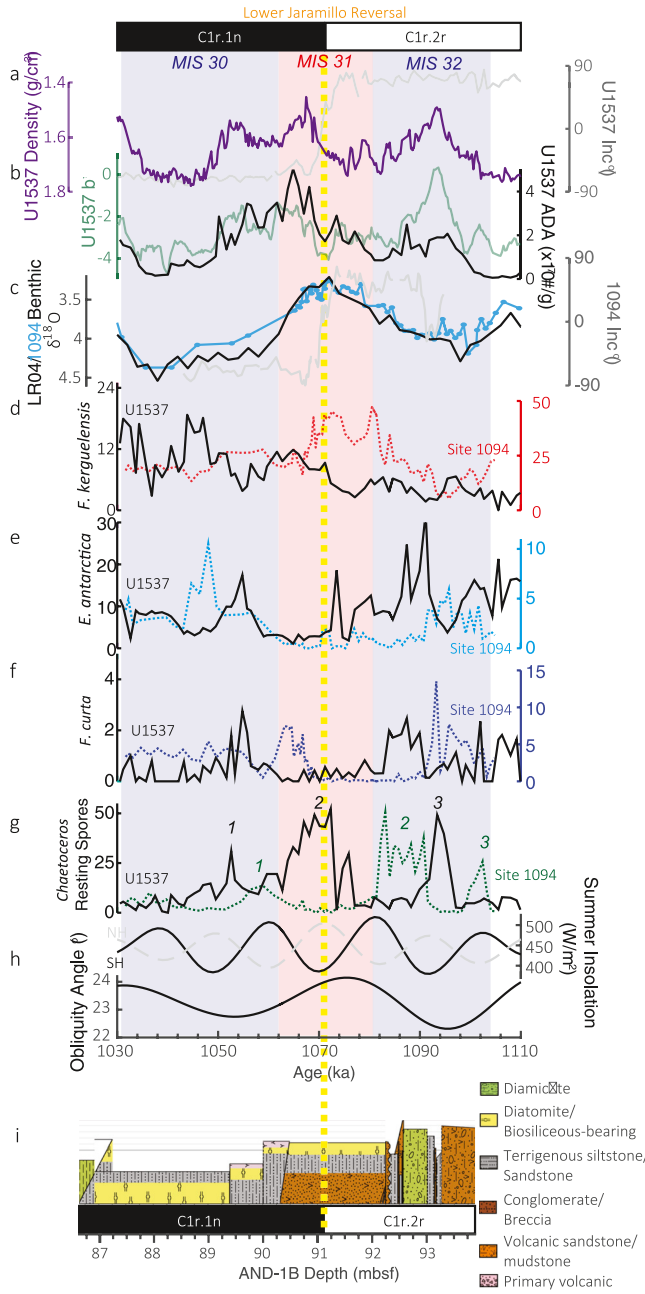

Figure 4. Comparison of U1537 (age model of Reilly et al., 2021), 1,094 (age model of Hasenfratz et al., 2019), and AND-1B (Naish et al., 2009; presented on its depth scale), with the position of the lower Jaramillo paleomagnetic reversal indicated by the vertical yellow dashed line (a) U1537 Density (low = more biogenic sediment; high = more lithogenic sediment) compared with paleomagnetic inclination (Reilly et al., 2021) (b) U1537 5-point smoothed b* (proportional to biogenic silica) compared with absolute diatom abundance (c) 1,094 Benthic $\delta^{18}O$ (blue; 25) and the LR04 stack (Lisiecki & Raymo, 2005) compared with 1,094 paleomagnetic inclination (Krissek et al., 2007) (d–g) Comparison of key U1537 (this study; solid lines) and 1,094 (Scherer et al., 2008; dashed lines) diatom species relative abundance (%): open ocean related *Fragilariopsis kerguelensis*, sea-ice associated *Eucampia antarctica and Fragilariopsis curta*, and primary productivity indicator *Chaetocerous* resting spores (h) Northern and Southern summer insolation and Earth's obliquity angle (Laskar et al., 2004) (a) Stratigraphic column for the lower Jaramillo interval at ANtarctic DRILLing-1B (modified from Krissek et al., 2007; Wilson et al., 2007; Villa et al., 2012).

loadings on PC1. The negative extreme on PC1 is *F. cylindrus*. The second PCA axis explains 20.6% of the variability in the data. The species with the most positive position on this axis is also *Th. lentiginosa,* followed by *E. antarctica, A. ingens,* and *Th. elliptipora*. The taxon with the most negative value for PC2 is CRS. The majority

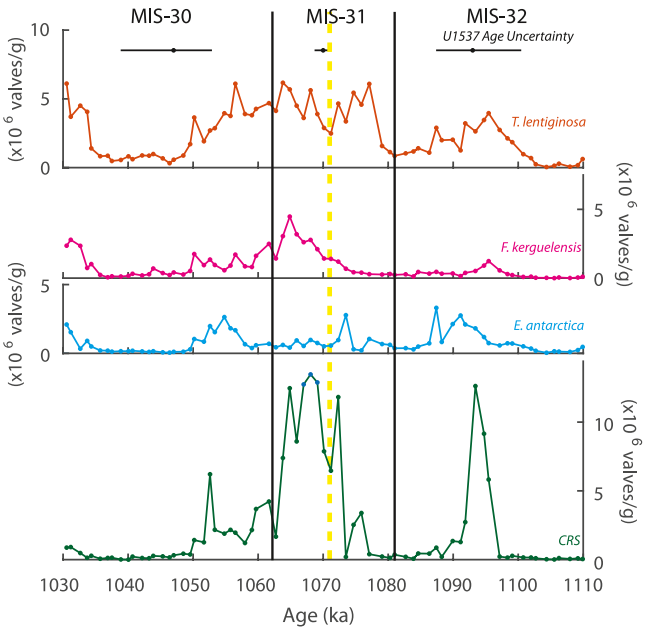

Figure 5. Diatom absolute abundance rates of chosen species. Absolute abundance rates (given as valves per gram dry weight of sediment) are given for selected diatom species. CRS = *Chaetoceros* resting spores.

of species cluster near the origin, and are slightly negative on axis 1 and slightly positive on axis 2 (Figure 2). The first two PCA axes are significant according to the broken stick model.

4. Discussion

4.1. Mechanisms of Warming

At Site U1537, MIS-31 is characterized by a decrease in the relative abundance of sea-ice affiliated diatoms (e.g., *E. antarctica* and *F. curta*; Figures 4e and 4f) coincident with increases in relative abundances of open ocean related diatom species (e.g., *F. kerguelensis, Th. elliptipora,* and *Th. lentiginosa*; Figures 3 and 4d). A reduction in sea-ice related species indicates a southward shift of the sea-ice edge, implying warmer surface waters. Furthermore, MIS-31 is represented by low density, diatom-dominated yellowish sediment, implying that the southern hemisphere westerlies have moved south of the core site at this time (Weber et al., 2022). The open ocean species that replace sea-ice species during this interval are found in higher abundance north of the sea-ice edge in the modern SO, further indicating warmer surface waters over the Site U1537 (Armand et al., 2005; Crosta et al., 2008; Esper et al., 2010; Leventer & Dunbar, 1996). In addition, increases in ADA correspond to warm intervals, implying warm productive water (Figure 3). *Chaetoceros* blooms are associated with warm SO waters and abundant nutrients, therefore, relative abundance of CRS (Figure 4g) also indicate warming (Crosta et al., 1997). These data support a WAIS mass reduction during MIS-31 as identified in other studies (McKay et al., 2012; Naish et al., 2009; Scherer et al., 1998, 2008).

PCA results support this alternation of warm and cold water environments. The primary PCA axis is constrained by warm-water, open ocean affiliated *Th. lentiginosa* (Crosta et al., 2005) on the positive side and the cold-water, sea-ice affiliated *F. cylindrus* (Armand et al., 2005, 2008) on the negative side (Figure 2). In addition, sea-ice affiliated species *A. actinochilus, F. curta, F. ritscheri,* and *F. separanda* cluster on the negative side of axis one (Armand et al., 2005, 2008). Open ocean affiliated species *F. kerguelensis* (Crosta et al., 2005), *A. ingens* and *Th. elliptopora* are also on the positive side of the axis. Therefore, PCA axis 1 is interpreted to represent a gradient of temperature and associated sea-ice conditions. Interestingly, open ocean associated *Th. oliverana* is on the negative side of the axis and sea ice affiliated *E. antarctica* is on the positive side of the axis. This may reflect a preference for proximity to the sea ice edge. *E antarctica* has previously been associated with sea ice edge habitats (Allen, 2014; Fryxell & Prasad, 1990). In addition, *T. oliverana position* is near *S. microtrias* on the PCA ordination space. *S. microtrias* has also been associated with sea-ice edge (Hasle et al., 1988) and sea-ice edge summer melt environments (Armand et al., 2008). Furthermore, *Th. oliverana* is known to achieve it's greatest relative abundance from the winter sea ice edge to the Antarctic Polar Front (Crosta et al., 2005).

Various mechanisms for warming are possible in the Southern Ocean, however orbitally paced, insolation-driven warming has been previously invoked (Scherer et al., 2008). Given that the duration of the examined interval, 1.030–1.110 Ma, is approximately the length of two obliquity cycles, robust spectral analysis to identify statistically significant frequencies in the obliquity or precession ranges is not possible. However, visual examination shows a plausible relationship between the relative abundance of *F. kerguelensis,* the most abundant diatom in the open ocean areas of the AZSO today (Armand et al., 2008; Crosta et al., 2005; Zielinski & Gersonde, 1997) and precession on the simple Site U1537 magnetostratigraphic age model (Figure 6). Specifically, *F. kerguelensis* relative abundance appears to follow a ~20 kyr pacing with the phase consistent with the mean daily insolation at 65°S for November 21st, that is, spring insolation, based on variation near the magnetic reversal at 1.071 Ma where the age model is strongest. This spring warmth would melt back the sea-ice edge, creating viable habitat for *F. kerguelensis*, thereby increasing its relative abundance. The increase in CRS abundance at the onset of this warming further indicates the presence of melt water (Crosta et al., 1997). *Fragilariopsis obliquecostata*, associated with summer sea-ice environments (Armand et al., 2005), was not present in any samples, implying the summer sea-ice edge was south of the Site, highlighting the importance of spring melt during this interval.

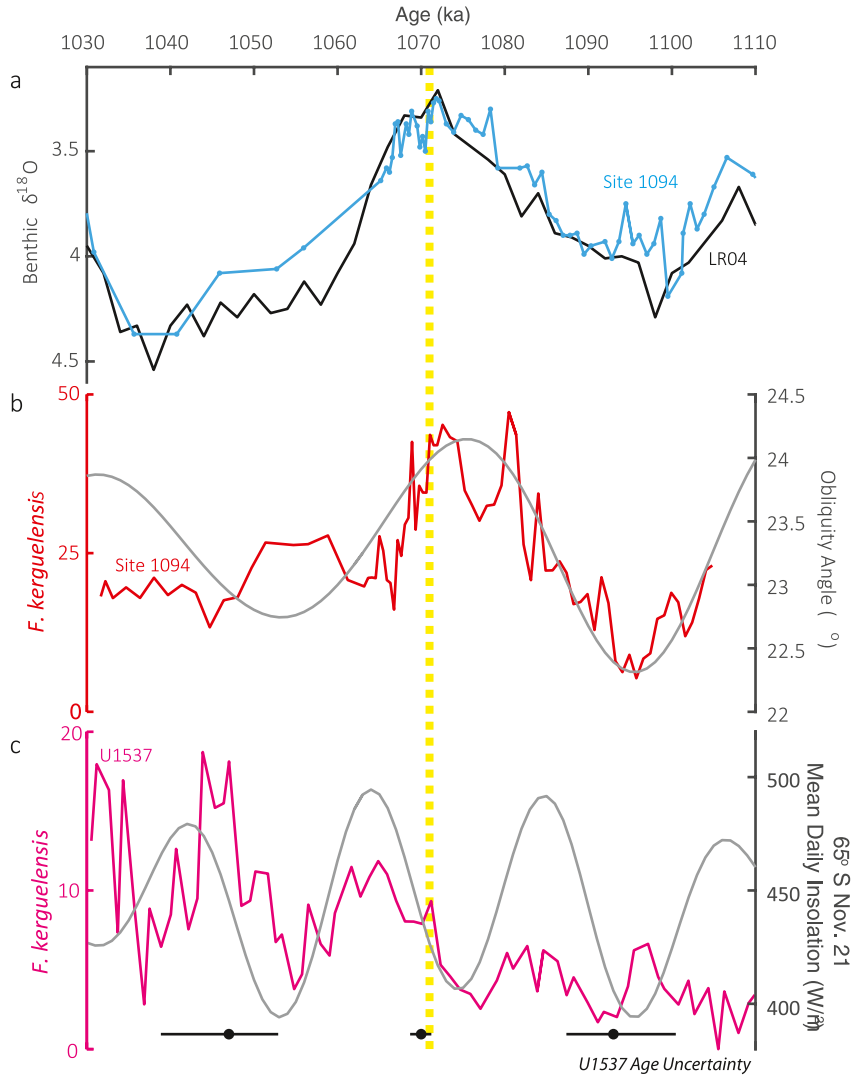

Figure 6. Orbital pacing of *Fragilariopsis kerguelensis* relative abundance through Marine Isotope Stage-31, compared with (a) bethic $\delta^{18}O$ and the lower Jaramillo reversal (yellow dashed line) (b) At Ocean Discovery Program (ODP) Site 1,094 (53°S) *F. kerguelensis* relative abundance varies with obliquity angle and the change in benthic $\delta^{18}O$ whereas at (c) IODP Site U1537 (59°S) *F. kerguelensis* relative abundance is paced by precession, highlighting the difference in orbital forcing between these different sectors of the Antarctic Zone of the Southern Ocean. ODP Site 1,094 diatom data are from Scherer et al. (6), with benthic $\delta^{18}O$ and age model from Hasenfratz et al. (2019). The LR04 stack is from Lisiecki and Raymo (2005) and orbital solutions are from Laskar et al. (2004). Diatom data are given as percent relative abundance.

The relative abundance of *F. kerguelensis* increases with each successive insolation maxima across MIS-31 and into MIS-30 (Figure 4c), indicating progressively earlier sea-ice retreat at Site U1537 with each precession cycle through MIS-31 that continued into MIS-30. This progressive sea-ice retreat would have brought relatively warm water nearer to the ice shelves and, consequently, help destabilizing the WAIS (Beltran et al., 2019; Pedro et al., 2016). The highest relative abundance of *F. kerguelensis* occurs after the lower Jaramillo paleomagnetic reversal at ~1.042 ± 0.008 Ma, indicating that the Scotia Sea may have remained warm during MIS-30.

Interestingly, open ocean affiliated *Th. lentiginosa* peaks consistently before *F. kerguelensis*. Furthermore, while the pattern of timing of peaks between *Th. lentiginosa* and *F. kerguelensis* is consistent, the magnitude differences are not. While each successive relative abundance peak of *F. kerguelensis* increases, *Th. lentiginosa* achieves a maximum relative abundance around 1.077 Ma. *Th. lentiginosa* requires lower nutrient availability than other open ocean affiliate species, notably *F. kerguelensis* (Armand et al., 2008). The most likely explanation of this similar yet contrasting abundance pattern is variability in available nutrients. PCA results support this conclusion.

Th. lentiginosa has the most positive value on PCA axis 2, where CRS, associated with high nutrient habitats, often stratified ice melt environments, have the most negative value (Leventer et al., 1996, 2002). Therefore, this axis is interpreted to represent variability in nutrients. Indeed, *F. kerguelensis,* which requires higher nutrient conditions than *Th. lentiginosa* is on the negative side of PC2 along with CRS. This implies that waters above U1537 warmed, resulting in an increase in *Th. lentiginosa* relative abundance increase, before nutrients became available to support *F. kerguelensis* and *Chaetoceros* spp. during each successive warming event. This progression implies the surface warms first, followed by increased nutrients from sea-ice melt, helping to explain the interglacially enhanced primary productivity seen here. While studies have shown an increase in iron (Fe mass accumulation rate), a limiting nutrient in the SO, resulting from dust deposition at the onset of MIS-30 in the subantarctic zone (Martínez-García et al., 2009), no such indication of dust-induced iron fertilization is present during late MIS-31 (Weber et al., 2022). Therefore, this nutrient source is likely from sea-ice melt.

4.2. Timing of Warming Across the Southern Ocean

At 53°S in Site 1,094, increases in open ocean related species and declines in sea-ice related species are also seen across MIS-31 (Scherer et al., 2008). However, comparison of the two sites shows a distinct difference in the timing of *F. kerguelensis* relative abundance increases and maxima (Figure 4d). The timing of the decline of sea-ice related species and increase in CRS are also asynchronous between the two sites (Figures 4e–4g). Furthermore, when placed on an updated benthic $\delta^{18}O$ chronology (Hasenfratz et al., 2019), visual examination shows a very close relationship between the increase in *F. kerguelensis* relative abundance, increase in obliquity, and the decrease in benthic $\delta^{18}O$ that defines the start of MIS-31 (Figure 6b). On orbital timescales, changes in the position and intensity of southern westerly wind (SWW) driven upwelling can be driven by global mean climate change and/or Earth's obliquity angle, with warmer global temperatures and lower obliquity angles both driving a poleward shift of the SWW and strengthening upwelling in the AZSO (Modes 1 and 3 of Ai et al., 2020). The increase in warm open water indicators, along with the decrease in benthic $\delta^{18}O$, suggests that oceanographic conditions at Site 1,094 were responding to the poleward shift of the SWW that occurred along with the mean global warming that occurred at the onset of MIS-31—different than our observations at Site U1537.

Although Site 1,094's chronology is well constrained through benthic $\delta^{18}O$ stratigraphy (Hasenfratz et al., 2019), the uncertainty of Site U1537's chronology increases with distance from the 1.071 Ma lower Jaramillo magnetic reversal, with estimated $\pm 1\sigma$ ranges growing to ~20 ka at the 1.030 and 1.110 Ma limits of our study interval (Reilly et al., 2021). Thus, our discussion of the pacing and phasing of these signals could change significantly if sedimentation rates were variable at Site U1537 through this time. For example, while the phase relationship between *F. kerguelensis* relative abundance and November 21st mean insolation at 65°S discussed earlier at Site U1537 is set by the timing of the *F. kerguelensis* abundance increase at the lower Jaramillo reversal, this relationship is only consistent with the preceding and following rises in insolation given age model uncertainty and not necessarily the actual phase relationship (see age uncertainty estimates in Figure 6). Furthermore, open ocean affiliated *Th. lentiginosa* shows the same relationship between abundance and insolation as *F. kerguelensis.* Nevertheless, there are differences between the initial onset of warmth at Sites 1,094 and U1537 that are robust to these kinds of age uncertainties due to their stratigraphic positions relative to the lower Jaramillo magnetic reversal. The maximum relative abundance of *F. kerguelensis*, and hence peak warmth conditions seen at Site 1,094, occurs during the ~10 kyr before the lower Jaramillo paleomagnetic reversal (Channell & Stoner, 2002; Scherer et al., 2008, Figure 6). At Site U1537 the maximum in *F. kerguelensis* relative abundance occurs after the lower Jaramillo paleomagnetic reversal. Therefore, despite the known age model uncertainties, the indication of peak warmth before (1,094, 53°S) and after (U1537, 59°S) the lower Jaramillo paleomagnetic reversal provides unequivocal evidence for a difference in timing of maximum warmth in the AZSO during MIS-31. This also indicates that the mechanisms that drive warmth in the southern regions of the AZSO are different than the more open northern AZSO, whether those mechanisms are related to local insolation forcing as we propose here or not. This is a significant finding for understanding WAIS mass loss and predicting future changes to the WAIS.

Analysis of sites further south provides additional evidence of time transgressive progression of peak warmth conditions following latitude across the Southern Ocean. Two drill sites in Southwestern Ross Sea, both at about 78°S, recovered a diatom-rich MIS-31; AND-1B (78°S; Naish et al., 2009) accumulated diatomite and diatom-rich volcaniclastic muds in relatively deep water, and CRP-1 (Bohaty et al., 1998) recovered diatom-rich sediments with abundant biogenic carbonate from a shallower bank. Both sites indicate ice shelf and ice sheet

retreat and the prevalence of open marine conditions from MIS-31 to MIS-27 (McKay et al., 2012; Naish et al., 2009; Scherer et al., 2007). Variable sedimentation rates in these more complicated, WAIS-proximal sediments prevent age model construction by linear interpolation between magnetic reversals in AND-1B and CRP-1, but there are no glacial overriding events, and open marine conditions associated with WAIS retreat from the Ross Sea area persisted, at least episodically, until the end of the Jaramillo subchron (0.988 Ma) (McKay et al., 2012). Marine diatoms emplaced within a volcaniclastic unit in AND-1B provide strong evidence for an absent or reduced Ross Ice Shelf prior to the lower Jaramillo paleomagnetic reversal (McKay et al., 2012). However, coccolithophore absolute abundance and species' relative abundance data (Villa et al., 2012), iceberg-rafted debris deposition (Teitler et al., 2015) and sedimentological indicators (McKay et al., 2012) from AND-1B indicate that peak warmth in the Ross Sea occurred after the lower Jaramillo paleomagnetic reversal, as seen at Site U1537 (Figure 4i). Peak warmth conditions are seen before the reversal at ODP Site 1,094 and after the reversal at U1537 and AND-1B, demonstrating that maximum warmth did not occur synchronously across the SO during MIS 31. Peak warm conditions are seen stratigraphically closer to the upper Jaramillo paleomagnetic reversal than the lower in the AND-1B drill site, whereas maximum warmth conditions are seen stratigraphically closer to the lower Jaramillo at Site U1537. Despite chronostratigraphic uncertainties in AND-1B, it is possible by using the globally synchronous time point of the lower Jaramillo magnetic reversal as comparison, therefore, that peak warmth conditions at the AND-1B drill site followed those seen at Site U1537.

Interestingly, the productivity indicator, %CRS, displays variability consistent with precession pacing at both Site 1,094 and Site U1537 (Figure 4g), but with different phasing. At both sites, %CRS typically increases around the transition from sea-ice dominated assemblages to open ocean assemblages, suggesting primary productivity at each site is strongest in sea-ice edge environment. This is consistent with the ecological preference of *Chaetoceros*, which bloom in well-stratified, nutrient-rich waters (Leventer et al., 1996; Leventer et al., 2002). At Site 1,094, CRS abundance correlates with SH summer insolation, whereas at Site U1537 CRS abundance apparently correlates with NH summer insolation. At Site 1,094, the largest CRS abundance peak occurs during the decrease in benthic $\delta^{18}O$ at the start of MIS-31, likely reflecting the intensification of SWW driven upwelling in the AZSO. Direct insolation forcing, paced by Earth's precession changes, melts the sea-ice edge while poleward shifts of the SWW provides warm, nutrient rich water in which CRS can bloom. Farther to the south in the AZSO at Site U1537, the influence of the precession paced local insolation driven sea-ice changes appear to be most dominant, while upwelling conditions may play a larger role at Site 1,094 in the more open northern AZSO (Figure 4g). Additionally, this may suggest that the latitudinal zone of primary productivity in the AZSO migrates between northerly and southerly locations in relation to expansion and contraction of the sea-ice edge on precessional timescales.

4.3. Nutrient Availability, Primary Productivity and Diatom Species' Absolute Abundances

Diatom absolute abundance data from Site U1537 indicate a strong contrast between glacial and interglacial conditions (Figure 5). With the exception of a brief increase in diatom absolute abundance during MIS-32, absolute abundance values are notably lower during glacials than interglacials, implying greater primary productive and diatom-bound carbon sequestration in marine sediments during MIS-31 than either MIS-32 or -30. This is in contrast to the 1,094 record where Martínez-García et al., 2009 found indications of increased rates of carbon burial (measured as total organic carbon mass accumulation rate) during glacials rather than interglacials, however, it supports results from Martinez-Garcia et al. (2011) and Jaccard et al. (2013) who found different glacial/interglacial patterns of primary productivity in the northern versus southern SO. Martínez-García et al. (2009) investigated ODP Site 1,090, located at approximately 42°55'S, whereas IODP Site U1537 is located at 59°S. This implies that primary productivity in the AZSO, south of the polar front, was decoupled from primary productivity north of the subantarctic front at this time as has been seen elsewhere (Martinez-Garcia et al., 2011; Jaccard et al., 2013; Weber et al., 2022). Sea-ice is the likely mechanism responsible for this decoupling. Site 1,090 would have been closer to the productive sea ice edge during a glacial than during an interglacial, when the sea ice edge and associated nutrients would have been much farther south (Cartagena-Sierra et al., 2021). Therefore, at this northern site favorable growth conditions for diatoms would have been present during glacials. The contrast in absolute abundance data from low glacial accumulation rates to high interglacial accumulation rates seen at more southerly Site U1537 implies the opposite. Site U1537 would have been covered by sea ice during glacial periods, greatly limiting primary productivity by blocking sunlight, whereas during interglacials favorable conditions would have existed over Site U1537. The brief peak in diatom absolute abundance identified

during MIS-32, dominated by CRS, implies a period of brief warmth allowing for primary productivity over Site U1537 around 1.093 Ma. This corresponds to a peak in magnetic susceptibility, that is, dust deposition, to the Site as well as a brief period of higher sea level (Weber et al., 2022). Unlike the typical pattern where dust and productivity are negatively correlated, this implies a brief warming event and corresponding dust deposition led to a spike in diatom primary productivity and associated carbon transport to the sea floor. Like diatom species relative abundance data described above, diatom species' absolute abundance data support a period of extended warmth following MIS-31 into early MIS-30. Unlike early MIS-32, where diatom absolute abundance values are near zero at the beginning of the glacial, absolute abundance values remain high into early MIS-30. While *F. kerguelensis* and CRS decline in absolute abundance fairly quickly into MIS-30, *Th. lentiginosa* maintains a higher absolute abundance longer. This implies that while warm conditions continued into early MIS-30 at Site U1537, nutrient availability declined more quickly. A short-lived peak in CRS is observed at ∼1.052 Ma, as *Th. lentiginosa* absolute abundance values are declining, implying a pulse of nutrients to the site. This productivity pulse could be associated with atmospheric dust deposition (Martínez-García et al., 2009; Weber et al., 2022).

Finally, diatom species' absolute abundances can be used to understand carbon burial in marine sediments. Although CRS are sometimes the most abundant diatom in a given sample, their very small size means their contribution to diatom-bound carbon sequestration may be minimal. However, both *F. kerguelensis* and *Th. lentiginosa,* the most abundant diatoms found throughout the analyzed interval excepting CRS, are considered to be heavy silica sinking species that bury carbon in marine sediments (Assmy et al., 2013). Furthermore, while *F. kerguelensis* is the most common open ocean diatom in the Southern Ocean (Armand et al., 2008; Crosta et al., 2005), *Th. lentiginosa* contributes more to carbon sequestration due to its larger size (Armand et al., 2008; Shukla et al., 2016). It is likely, therefore, that carbon burial at Site U1537 was high throughout MIS-31 where *Th. lentiginosa* absolute abundance is high. The rate of carbon burial would have increased late in MIS-31 as the absolute abundance of *F. kerguelensis* increased and remained somewhat high through the first half of MIS-30. This is further indicated by the very high CRS abundance during later MIS-31 (Abelmann et al., 2006). As above, this is in contrast to Martínez-García et al. (2009) who found carbon burial to be higher during glacials than interglacials. However, this pattern of contrast in carbon burial between the Antarctic Zone (higher carbon deposition during interglacials) and Subantarctic Zone (higher carbon deposition during glacials) has been identified over the last glacial cycle (Jaccard et al., 2013). Kohfeld et al. (2005) also found primary productivity to be higher during the Holocene and MIS-5a-d than the LGM south of the polar front, but the opposite north of the polar front. Further support comes from Weber et al. (2022), who observed this same relationship, higher primary productivity and carbon burial during interglacials relative to glacials south of the polar front, to be consistent over the last 1.5 Ma. Our data corroborate these studies showing a N-S difference relative to the polar front in ideal conditions for carbon burial, that is, variations in iron availability and the light-limiting effect of sea-ice cover north and south of the polar front, existed in the SO during MIS-32 to -30. This further highlights the importance of creating multiple reconstructions of carbon deposition rates across the polar front for any given time period to accurately understand the SO's role in the global carbon cycle.

5. Conclusions

Comparison of the diatom records of ODP Site 1,094 and IODP Site U1537 reveals a more complex evolution of warmth across the AZSO during MIS-31 than has been previously postulated. While more quantitative analysis is limited by age model uncertainty, we find that during MIS-31 warming follows obliquity and the decrease in benthic $\delta^{18}O$ in the northern sector of the AZSO, while warming is delayed and potentially paced by local insolation, that is, precession, in the southern sector. This evidence for local SH-precessional forcing means that paleoceanographic changes recorded at Site U1537 differ in timing and cyclicity from the global average $\delta^{18}O$ ice volume signal, and may provide supporting evidence for the antiphase hypothesis (Raymo et al., 2006). Taken together with findings from AND-1B and CRP-1 (McKay et al., 2012; Scherer et al., 2007, 2008; Villa et al., 2012), these data from Site U1537 imply that warming in the southern region of the AZSO was driven by local radiative forced sea-ice loss late in MIS-31. This is contrasted with the change in zonal wind strength and associated warm water upwelling that drove the previously described warming in the northern AZSO in early MIS-31. Thus, the locally driven precession paced insolation forcing may have been the major driver for ice shelf retreat and subsequent ice sheet collapse in Antarctica. The lack of an obvious decrease in global $\delta^{18}O$ record could be explained by coeval growth of NH icesheets (e.g., the anti-phase hypothesis, Raymo et al., 2006).

This interpretation is consistent with modeling results that indicate the importance of local oceanographic forcing for ice retreat during this interval (DeConto et al., 2012). Although previous studies have revealed differences in orbital response in the Subantarctic and Antarctic zones of the Southern Ocean (Jaccard et al., 2013), the results presented here reveal different responses to orbital forcing within the AZSO itself. While there is still uncertainty in the precise pacing of *F. kerguelensis* relative abundance at Site U1537, the timing and duration of these warm ocean indicators are distinctly different between the two sites, providing unequivocal evidence of a latitudinal difference in the mechanisms of sea surface warming. This is the first evidence of different mechanisms of warmth acting in the Northern versus Southern Zones of the AZSO, a significant finding for understanding and predicting the behavior of the Antarctic Ice Sheets.

Peak warm conditions are seen prior to the lower Jaramillo paleomagnetic reversal in the northern regions of the Southern Ocean (Site 1,094), but subsequent to this time marker further to the south (Site U1537 and AND-1B). The lower Jaramillo paleomagnetic reversal allows for a robust relative chronology demonstrating this difference, despite the lack of linear sedimentation rate and high-resolution age model at AND-1B. This is a significant result for building accurate models of warming in the SO. Although the drivers of anthropogenic warming are related to greenhouse gas emissions, and thus notably different from the orbitally forced climate change that occurred during MIS-31, that is, anthropogenic greenhouse gas emissions compared to orbital forcing, these results highlight the importance of southward migration of warming water masses in the Southern Ocean for destabilizing the modern WAIS.

Lastly, comparison of diatom species' absolute abundances provides support for an extended warm period during early MIS-30 at Site U1537. Diatom absolute abundance data also show the greatest carbon burial during interglacials, with low diatom absolute abundance during glacials. This is in contrast to sites farther north, where carbon transport to the seafloor is higher during glacial periods. These results demonstrate the importance of reconstructing diatom absolute abundances across the Southern Ocean to understand their role in the global carbon cycle.

Data Availability Statement

Data generated for this work, diatom relative and absolute abundance data, are available in the supplemental materials and at Pangaea (Warnock, 2022).

Acknowledgments
We would like to thank the crew and science staff of the *JOIDES Resolution* for their hard work. Without them this work would not be possible. Warnock, Reilly, and the US participants on IODP Expedition 382 received support from post expedition awards though the US Science Support Program and Columbia University (NSF award OCE 1450528). Scherer is supported by NSF award ANT1939146. Warnock, Reilly, Williams, Bailey, Brachfeld, Hemming, O'Connell, and Tauxe are supported through a collaborative award through NSF Office of Polar Programs (2114769, 2114764, 2114777, 2114786, 2114768, 2114763). M. E. Weber received funding by the Deutsche Forschungsgemeinschaft (DFG–Priority Programme 527, Grant We2039/17–1). L. F. Pérez was funded by the European Union's Horizon 2020 Marie Skłodowska-Curie grant agreement No. 792773 WAMSISE and the Natural Environment Research Council (NERC) UK-IODP programme grand NEB1782. L. Armbrecht is funded by the Australian and New Zealand International Ocean Discovery Program Consortium (ANZIC) and an Australian Research Council (ARC) Discovery Early Career Researcher Award (DECRA) (DE210100929). I. Bailey thanks the Natural Environmental Research Council for financial support for his participation in IODP Exp. 382 and for associated post-expedition research (UK IODP grant NE/T006609/1). Scherer is funded by NSF ANT1939139. We thank Adam Hasenfratz for helpful discussion on the stratigraphy of ODP Site 1,094. JW dedicates this work to the memory of Southern Ocean diatom specialist Dr. Leanne Armand, mentor, inspiration and friend.

References

Abelmann, A., Gersonde, R., Cortese, G., Kuhn, G., & Smetacek, V. (2006). Extensive phytoplankton blooms in the Atlantic sector of the glacial Southern Ocean. *Paleoceanography*, *21*(1), PA1013. https://doi.org/10.1029/2005PA001199

Ai, X. E., Studer, A. S., Sigman, D. M., Martínez-García, A., Fripiat, F., Thöle, L. M., et al. (2020). Southern Ocean upwelling, Earth's obliquity, and glacial-interglacial atmospheric CO_2 change. *Science*, *370*(6522), 1348–1352. https://doi.org/10.1126/science.abd2115

Allen, C. A. (2014). Proxy development: A new facet of the morphological diversity in the marine diatom *Eucampia antarctica* (castracane) mangin. *Journal of Micropaleontology*, *33*(2), 131–142. https://doi.org/10.1144/jmpaleo2013-025

Amante, C., & Eakins, B. W. (2009). *ETOPO1 1 arc-minute global relief model: Procedures, data sources and analysis*. National Geophysical Data Center, NOAA. NOAA Technical Memorandum NESDIS NGDC-24. https://doi.org/10.7289/V5C8276M

Anderson, J. B., & Andrews, J. T. (1999). Radiocarbon constraints on ice sheet advance and retreat in the Weddell Sea, Antarctica. *Geology*, *27*(2), 179–182. https://doi.org/10.1130/0091-7613(1999)027<0179:rcoisa>2.3.co;2

Armand, L. K., Crosta, X., Quéguiner, B., Mosseri, J., & Garcia, N. (2008). Diatoms preserved in surface sediments of the northeastern Kerguelen Plateau. *Deep-Sea Research II*, *55*(5–7), 677–692. https://doi.org/10.1016/j.dsr2.2007.12.032

Armand, L. K., Crosta, X., Romero, O., & Pichon, J.-J. (2005). The biogeography of major diatom taxa in Southern Ocean sediments: 1. Sea-Ice related species. *Palaeogeography, Palaeoclimatology, Palaeoecology*, *223*(1–2), 93–126. https://doi.org/10.1016/j.palaeo.2005.02.015

Arndt, J. E., Schenke, H. W., Jakobsson, M., Nitsche, F. O., Buys, G., Goleby, B., et al. (2013). The international bathymetric chart of the Southern Ocean (IBCSO) Version 1.0—A new bathymetric compilation covering circum-Antarctic waters. *Geophysical Research Letters*, *40*(12), 3111–3117. https://doi.org/10.1002/grl.50413

Assmy, P., Smetacek, V., Montresor, M., Klass, C., Henjes, J., Strass, V. H., et al. (2013). Thick-shelled, grazer-protected diatoms decouple ocean carbon and silicon cycles in the iron-limited Antarctic Circumpolar Current. *Proceedings of the National Academy of Sciences of the Unites States of America*, *110*(51), 20633–20638. https://doi.org/10.1073/pnas.1309345110

Beltran, C., Golledge, N. R., Christian, O., Kowalewski, D. E., Sicre, M.-A., Hageman, K. J., et al. (2019). Southern Ocean temperature records and ice-sheet models demonstrate rapid Antarctic ice sheet retreat under low atmospheric CO_2 during Marine Isotope Stage 31. *Quaternary Science Reviews*, *228*, 106069. https://doi.org/10.1016/j.quascirev.2019.106069

Bohaty, S. M., Scherer, R. P., & Harwood, D. M. (1998). Lower Pleistocene diatom biostratigraphy of the CRP-1 diatomite. *Terra Antarctica*, *5*, 431–454.

Budge, J. S., & Long, D. G. (2018). A comprehensive database for Antarctic Iceberg tracking using scatterometer data. *IEEE Journal of Selected Topics in Applied Earth Observations and Remote Sensing*, *11*(2), 434–442. https://doi.org/10.1109/jstars.2017.2784186

Cartagena-Sierra, A., Berke, M. A., Robinson, R. S., Marcks, B., Castañeda, I. S., Starr, A., et al. (2021). Latitudinal migrations of the subtropical front at the agulhas plateau through the mid-pleistocene transition. *Paleoceanography and Paleoclimatology*, *36*(7), e2020PA004084. https://doi.org/10.1029/2020pa004084

Channell, J. E. T., Hodell, D. A., Xuan, C., Mazaud, A., & Stoner, J. S. (2008). Age calibrated relative paleointensity for the last 1.5 Myr at IODP site U1308 (North Atlantic). *Earth and Planetary Science Letters*, *274*(1–2), 59–71. https://doi.org/10.1016/j.epsl.2008.07.005

Channell, J. E. T., & Stoner, J. S. (2002). Plio-Pleistocene magnetic polarity stratigraphies and diagenetic magnetite dissolution at ODP Leg 177 Sites (1089, 1091, 1093, 1094). *Marine Micropaleontology*, *45*(3–4), 269–290. https://doi.org/10.1016/s0377-8398(02)00032-4

Crosta, X., Denis, D., & Ther, O. (2008). Sea ice seasonality during the Holocene, adélie land, East Antarctica. *Marine Micropalentology*, *66*(3–4), 222–232. https://doi.org/10.1016/j.marmicro.2007.10.001

Crosta, X., Pichon, J.-J., & Labracherie, M. (1997). Distribution of *Chaetoceros* resting spores in modern peri-Antarctic sediments. *Marine Micropalentology*, *29*(3–4), 283–299. https://doi.org/10.1016/s0377-8398(96)00033-3

Crosta, X., Romero, O., Armand, L. K., & Pichon, J.-J. (2005). The biogeography of major diatom taxa in Southern Ocean sediments: 2. Open ocean related species. *Palaeogeography, Palaeoclimatology, Palaeoecology*, *223*(1–2), 66–92. https://doi.org/10.1016/j.palaeo.2005.03.028

DeConto, R. M., Pollard, D., & Kowalewski, D. (2012). Modeling Antarctic ice sheet and climate variations during Marine Isotope Stage 31. *Global and Planetary Change*, *96–97*, 181–188. https://doi.org/10.1016/j.gloplacha.2012.03.003

Elderfield, H., Ferretti, P., Greaves, M., Crowhurst, S., McCave, I. N., Hodell, D., & Piotrowski, A. M. (2012). Evolution of ocean temperature and ice volume through the mid-pleistocene climate transition. *Science*, *337*(6095), 704–709. https://doi.org/10.1126/science.1221294

Esper, O., Gersonde, R., & Kadagies, N. (2010). Diatom distribution in southeastern Pacific surface sediment and their relationship to modern environmental variables. *Palaeogeography, Palaeoclimatology, Palaeoceanography*, *287*(1–4), 1–21. https://doi.org/10.1016/j.palaeo.2009.12.006

Fryxell, G. A., & Prasad, A. K. S. K. (1990). Eucampia Antarctica var. recta (Mangin) stat. nov. (Biddulphiaceae, Bacillariophyceae): Life stages at the Weddell Sea ice edge. *Phycologia*, *29*(1), 27–38. https://doi.org/10.2216/i0031-8884-29-1-27.1

Gilbert, E., & Kittel, C. (2021). Surface melt and runoff on Antarctic ice shelves at 1.5°C, 2°C and 4°C of future warming. *Geophysical Research Letters*, *48*(8). https://doi.org/10.1029/2020GL091733

Hammer, Ř., Harper, D. A. T., & Ryan, P. D. (2001). PAST: Paleontological statistics software package for education and data analysis. *Palaeontologia Electronica*, *4*(1), 9.

Hasenfratz, A. P., Jaccard, S. J., Martínez-García, A., Sigman, D. M., Hodell, D. A., Vance, D., et al. (2019). The residence time of Southern Ocean surface waters and the 100, 000-year ice age cycle. *Science*, *363*(6431), 1080–1084. https://doi.org/10.1126/science.aat7067

Hasle, G. R., Sims, P. A., & Syvertsen, E. E. (1988). Two recent *Stellarima* species: *S. Microtrias* and *S. stellaris* (bacillariophyceae). *Botanica Marina*, *31*(3), 195–206. https://doi.org/10.1515/botm.1988.31.3.195

Hönisch, B., Hemming, N. G., Archer, D., Siddall, M., & McManus, J. (2009). Atmospheric carbon dioxide concentration across the Mid-Pleistocene Transition. *Science*, *324*(5934), 1551–1554. https://doi.org/10.1126/science.1171477

Horng, C.-S., Lee, M.-Y., Pälike, H., Wei, K.-Y., Liang, W.-T., Iizuka, Y., & Torii, M. (2002). Astronomically calibrated ages for geomagnetic reversals within the Matuyama chron. *Earth Planets and Space*, *54*(6), 679–690. https://doi.org/10.1186/bf03351719

Huybers, P. (2006). Early Pleistocene glacial cycles and the integrated summer insolation forcing. *Science*, *313*(5786), 508–511. https://doi.org/10.1126/science.1125249

Jaccard, S. L., Hayes, C. T., Martínez-García, A., Hodell, D. A., Anderson, R. F., Sigman, D. M., & Haug, G. H. (2013). Two modes of change in Southern Ocean productivity over the past million years. *Science*, *339*(6126), 1419–1423. https://doi.org/10.1126/science.1227545

Kohfeld, K. E., Le Quere, C., Harrison, S. P., & Anderson, R. F. (2005). Role of marine biology in glacial-interglacial CO2 cycles. *Science*, *308*(5718), 74–78.

Krissek, L., Browne, G., Carter, L., Cowan, E., Dunbar, G., McKay, R., et al. (2007). Sedimentology and stratigraphy of the AND-1B core, ANDRILL McMurdo ice shelf project, Antarctica. *Terra Antartica*, *14*(3), 185–222.

Laskar, J., Robutel, P., Joutel, F., Gastineau, M., Correia, A. C. M., & Levrard, B. (2004). A long-term numerical solution for the insolation quantities of the Earth. *Astronomy and Astrophysics*, *428*(1), 261–285. https://doi.org/10.1051/0004-6361:20041335

Leventer, A., Domack, E., Barkoukis, A., McAndrews, B., & Murray, J. (2002). Laminations from the palmer deep: A diatom-based interpretation. *Paleoceanography*, *17*(2), PAL3-1–PAL3-15. https://doi.org/10.1029/2001PA000624

Leventer, A., Domack, E. W., Ishman, S. E., Brachfeld, S., McClennen, C. E., & Manley, P. (1996). Productivity cycles of 200-300 years in the Antarctic Peninsula region: Understanding linkages among the sun, atmosphere, oceans, sea-ice, and biota. *The Geological Society of America Bulletin*, *108*(12), 1626–1644. https://doi.org/10.1130/0016-7606(1996)108<1626:pcoyit>2.3.co;2

Leventer, A., & Dunbar, R. B. (1996). Factors influencing the distribution of diatoms and other algae in the Ross Sea. *Journal of Geophysical Research*, *101*(C8), 18489–18500. https://doi.org/10.1029/96jc00204

Lisiecki, L. E., & Raymo, M. E. (2005). A Pliocene-Pleistocene stack of 57 globally distributed benthic δ18O records. *Paleoceanography*, *20*(1), PA1003. https://doi.org/10.1029/2004pa001071

Liu, H., Jezek, K. C., Li, B., & Zhao, Z. (2015). *Radarsat Antarctic mapping project digital elevation model, Version 2*. NASA National Snow and Ice Data Center Distributed Active Archive Center. https://doi.org/10.5067/8JKNEW6BFRVD

Lougheed, B., & Obrochta, S. (2019). A rapid, deterministic age-depth modeling routine for geological sequences with inherent depth uncertainty. *Paleoceanography and Paleoclimatology*, *34*(1), 122–133. https://doi.org/10.1029/2018PA003457

Maiorano, P., Marino, M., & Flores, A. (2009). The warm interglacial marine isotope stage 31: Evidences from the calcareous nannofossil assemblages at ODP site 1090 (Southern Ocean). *Marine Micropalentology*, *71*(3–4), 166–175. https://doi.org/10.1016/j.marmicro.2009.03.002

Maldonado, A., Bohoyo, F., Galindo-Zaldívar, J., Hernández-Molina, F. J., Lobo, F. J., Lodolo, E., et al. (2014). A model of oceanic development by ridge jumping: Opening of the Scotia Sea. *Global and Planetary Change*, *123*, 152–173. https://doi.org/10.1016/j.gloplacha.2014.06.010

Martínez-García, A., Rosell-Melé, A., Geibert, W., Gersonde, R., Masqué, P., Gaspari, V., & Barbante, C. (2009). Links between iron supply, marine productivity, sea surface temperature, and CO_2 over the last 1.1 Ma. *Paleoceanography*, *24*(1). https://doi.org/10.1029/2008PA001657

Martinez-Garcia, A., Rosell-Mele, A., Jaccard, S. L., Geibert, W., Sigman, D. M., & Haug, G. H. (2011). Southern Ocean dust-climate coulpling over the past four million years. *Nature*, *476*, 312–315.

Matsuoka, K., Skoglund, A., Roth, G., de Pomereu, J., Griffiths, H., Headland, R., et al. (2021). Quantarctica, an integrated mapping environment for Antarctica, the Southern Ocean, and sub-Antarctic islands. *Environmental Modelling & Software*, *140*, 105015. https://doi.org/10.1016/j.envsoft.2021.105015

McKay, R., Naish, T., Carter, L., Powell, R., Barrett, P., Scherer, R., et al. (2012). Pleisocene variability of Antarctic ice sheet extent in the Ross embayment. *Quaternary Science Reviews*, *34*, 93–112. https://doi.org/10.1016/j.quascirev.2011.12.012

Melles, M., Brigham-Grette, J., Minyuk, P. S., Nowaczyk, N. R., Wennrich, V., DeConto, R. M., et al. (2012). 2.8 million years of Arctic climate change from Lake El'gygytgyn, NE Russia. *Science*, *337*(6092), 315–320. https://doi.org/10.1126/science.1222135

Morlighem, M., Rignot, E., Binder, T., Blankenship, D., Drews, R., Eagles, G., et al. (2020). Deep glacial troughs and stabilizing ridges unveiled beneath the margins of the Antarctic ice sheet. *Nature Geoscience*, *13*(2), 132–137. https://doi.org/10.1038/s41561-019-0510-8

Naish, T., Powell, R., Levy, R., Wilson, G., Scherer, R., Talarico, F., et al. (2009). Obliquity-paced Pliocene west Antarctic ice sheet oscillation. *Nature*, *458*(7236), 322–328. https://doi.org/10.1038/nature07867

Nakayama, Y., Oshima, K. I., Matsumara, Y., Fukamachi, Y., & Hasumi, H. (2014). A numerical investigation of formation and variability of Antarctic bottom water off Cape Darnley, East Antarctica. *Journal of Physical Oceanography*, *44*(11), 2921–2937. https://doi.org/10.1175/jpo-d-14-0069.1

Orsi, A. H., Whitworth, T., III, & Nowlin, W. D., Jr. (1995). On the meridional extent and fronts of the Antarctic Circumpolar Current. *Deep-Sea Research*, *42*(5), 641–673. https://doi.org/10.1016/0967-0637(95)00021-w

Pedro, J. B., Martin, T., Steig, E. J., Jodhum, M., Park, W., & Rasmussen, S. O. (2016). Southern Ocean deep convection as a driver of Antarctic warming events. *Geophysical Research Letters*, *43*(5), 2192–2199. https://doi.org/10.1002/2016gl067861

Pérez, L. F., Martos, Y. M., García, M., Weber, M. E., Raymo, M. E., Williams, T., et al. (2021). Miocene to present oceanographic variability in the Scotia Sea and Antarctic ice sheets dynamics: Insight from revised seismic-stratigraphy following IODP Expedition 382. *Earth and Planetary Science Letters*, *553*, 116657. https://doi.org/10.1016/j.epsl.2020.116657

Raymo, M. E., Lisiecki, L. E., & Nisancioglu, K. H. (2006). Plio-pleistocene ice volume, Antarctic climate, and the global δ18O record. *Science*, *313*(5786), 492–495. https://doi.org/10.1126/science.1123296

Reilly, B. T., Tauxe, L., Brachfeld, S., Raymo, M., Bailey, I., Hemming, S., et al. (2021). New magnetostratigraphic insights from iceberg Alley on the rhythms of Antarctic climate during the plio-pleistocene. *Paleoceanography and Paleoclimatology*, *36*(2), e2020PA003994. https://doi.org/10.1029/2020PA003994

Rignot, E., Jacobs, S., Mouginot, J., & Scheuchl, B. (2013). Ice-shelf melting around Antarctica. *Science*, *341*(6143), 266–270. https://doi.org/10.1126/science.1235798

Romero, O. E., Armand, L. K., Crosta, X., & Pichon, J.-J. (2005). The biogeography of major diatom taxa in Southern Ocean surface sediments: 3. Tropical/subtropical species. *Palaeogeography, Palaeoclimatology, Palaeoecology*, *223*(1–2), 49–65. https://doi.org/10.1016/j.palaeo.2005.03.027

Scherer, R., Hannah, M., Maffioli, P., Persico, D., Sjunneskog, C., Strong, C. P., et al. (2007). Palaeontologic characterisation and analysis of the AND-1B core, ANDRILL McMurdo ice shelf project, Antarctica. *Terra Antarctica*, *14*(3), 223–254.

Scherer, R. P., Aldahan, A., Tulaczyk, S., Possnert, G., Engelhardt, H., & Kamb, B. (1998). Pleistocene collapse of the west Antarctic ice sheet. *Science*, *281*(5373), 82–85. https://doi.org/10.1126/science.281.5373.82

Scherer, R. P., Bohaty, S. M., Dunbar, R. B., Esper, O., Flores, J.-A., Gersonde, R., et al. (2008). Antarctic records of precession-paced insolation-driven warming during early Pleistocene Marine Isotope Stage 31. *Geophysical Research Letters*, *35*(3), L03505. https://doi.org/10.1029/2007gl032254

Seroussi, H., Nakayama, Y., Menemenlis, D., Morlighem, M., Rignot, E., & Khazendar, A. (2017). Continued retreat of Thwaites Glacier, West Antarctica, controlled by bed topography and ocean circulation. *Geophysical Research Letters*, *44*(12), 6191–6199. https://doi.org/10.1002/2017gl072910

Shackleton, N. J., Berger, A., & Peltier, W. R. (1990). An alternative astronomical calibration of the lower Pleistocene timescale based on ODP Site 677. *Earth and Environmental Science Transactions of the Royal Society of Edinburgh*, *81*(4), 251–261. https://doi.org/10.1017/s0263593300020782

Shukla, S. K., Crespin, J., & Crosta, X. (2016). *Thalassiosira lentiginosa* size variation and associated biogenic silica burial in the Southern Ocean over the last 42 kyrs. *Marine Micropaleontology*, *127*, 74–85. https://doi.org/10.1016/j.marmicro.2016.07.006

Spreen, G., Kaleschke, L., & Heygster, G. (2008). Sea-ice remote sensing using AMSR-E 89 GHz channels. *Journal of Geophysical Research*, *113*(C2), C02S03. https://doi.org/10.1029/2005JC003384

Teitler, L., Florindo, F., Warnke, D. A., Filippelli, G. M., Kupp, G., & Taylor, B. (2015). Antarctic Ice sheet response to a long warm interval across marine isotope stage 31: A cross-latitudinal study of iceberg-rafted debris. *Earth and Planetary Science Letters*, *409*, 109–119. https://doi.org/10.1016/j.epsl.2014.10.037

Villa, G., Lupi, C., Cobianchi, M., Florindo, F., & Pekar, S. F. (2008). A pleisotcene warming event at 1 Ma in Prydz Bay, East Antarctica: Evidence from ODP site 1165. *Palaeogeography, Palaeoclimatology, Palaeoecology*, *260*(1–2), 230–244. https://doi.org/10.1016/j.palaeo.2007.08.017

Villa, G., Persico, D., Wise, S., & Gadaleta, A. (2012). Calcareous nannofossil evidence for marine isotope stage 31 (1 Ma) in core AND-1B, ANDRILL McMurdo ice shelf project (Antarctica). *Global and Planetary Change*, *96–97*, 75–86. https://doi.org/10.1016/j.gloplacha.2009.12.003

Warnock, J. P. (2022). Diatom relative and absolute abundances from IODP Site U1537 covering MIS-32 to -29 collected via light microscopy. [Dataset]. https://doi.org/10.1594/PANGAEA.946624

Warnock, J. P., & Scherer, R. P. (2014). A revised method for determining the absolute abundance of diatoms. *Journal of Paleolimnology*, *53*(1), 157–163. https://doi.org/10.1007/s10933-014-9808-0

Weber, M. E., Bailey, I., Hemming, S. R., Martos, Y. M., Reilly, B. T., Ronge, T. A., et al. (2022). Antiphased dust deposition and productivity in the Antarctic Zone over 1.5 million years. *Nature Communications*, *13*(1), 2044. https://doi.org/10.1038/s41467-022-29642-5

Weber, M. E., Clark, P. U., Kuhn, G., Timmermann, A., Sprenk, D., Gladstone, R., et al. (2014). Millennial-scale variability in Antarctic ice-sheet discharge during the last deglaciation. *Nature*, *510*(7503), 134–137. https://doi.org/10.1038/nature13397

Weber, M. E., Kuhn, G., Sprenk, D., Rolf, C., Ohlwein, C., & Ricken, W. (2012). Dust transport from Patagonia to Antarctica – A new stratigraphic approach from the Scotia Sea and its implications for the last glacial cycle. *Quaternary Science Reviews*, *36*, 177–188. https://doi.org/10.1016/j.quascirev.2012.01.016

Weber, M. E., Raymo, M. E., Peck, V. L., Williams, T., & The Expedition 382 Scientists. (2021). *Iceberg Alley and subantarctic ice and ocean dynamics*. Proceedings of the International Ocean Discovery Program, 382, (International Ocean Discovery Program). https://doi.org/10.14379/iodp.proc.382.2021

Wilson, G., Levy, R., Browne, G., Cody, R., Dunbar, N., Florindo, F., et al. (2007). Preliminary integrated chronostratigraphy of the AND-1B core, ANDRILL McMurdo ice shelf project, Antarctica. *Terra Antarctica*, *14*(3), 297–316.

Zielinski, U., & Gersonde, R. (1997). Diatom distribution in Southern Ocean surface sediments (Atlantic sector): Implications for paleoenvironmental reconstructions. *Palaeogeography, Palaeoclimatology, Palaeoecology*, *129*(3–4), 213–250. https://doi.org/10.1016/s0031-0182(96)00130-7